RSC Advances

PAPER

View Article Online
View Journal | View Issue

Cite this: *RSC Adv.*, 2015, **5**, 71472

Solar light based degradation of organic pollutants using ZnO nanobrushes for water filtration†

Ankur Gupta,‡ Jayant Raj Saurav‡ and Shantanu Bhattacharya*

In this work, we report an effective water filtration system based on the photocatalytic performance of semiconducting dense nano-brushes under natural sunlight. During thin-film photocatalysis, which is usually performed by a deposited layer of photocatalyst, a stagnant boundary layer is created near the catalyst which adversely affects the rate of adsorption because of diffusional restrictions. One strategy that may be used is to disrupt this laminar boundary layer by creating a super-dense nanostructure near the surface of the catalyst. Furthermore, it is useful to fabricate a structured filter element for the passage of water with the use of nanostructures protruding out of the surface. Herein, dye remediation is performed by solar means. This remediation was initially limited to a lower efficiency because of diffusional restrictions but has now become a fast process due to microhole incorporation in the filter materials with protruding dense nanostructures. Theoretical analysis predicts that there is an optimal film thickness that yields the maximum adsorption and also a highly nonlinear behaviour of diffusivity with respect to the fraction adsorbed. The effect of increased surface area due to microholes on the fraction adsorbed is also investigated and it is found that there is an optimum value of hole diameter for maximum adsorption.

Received 2nd June 2015
Accepted 7th August 2015

DOI: 10.1039/c5ra10456d

www.rsc.org/advances

1. Introduction

Environmental contaminants like pesticides, dyes and heavy metals in water require remediation and possible removal to make the water fit for human consumption. A lot of research is prevalent to purify water from its contaminants, a major portion of which are organic in nature. Further, the photocatalytic degradation of organic pollutants from water using semiconducting materials has attracted a lot of attention. Such semiconductors are increasingly used for oxidation or degradation of organic dyes and other contaminants particularly in industrial wastewater. The basic mechanism for this remediation is primarily based on the oxygen defects on the surface of the semiconducting materials which when activated by photon irradiation are used to destroy the organic contaminants. The various advantages that the process has are (a) the photocatalytic reaction is not specific to compounds and, therefore, is capable of destroying a spectrum of organic chemicals like hydrocarbon fuels, halogenated solvents, surfactants, pesticides and many hazardous organic chemicals,[1,2] (b) this process is very effective mostly owing to the process of its removal, often achieving a complete degradation, (c) the process is very resistant to toxicity *etc.*, (d) the process can be applied equally well to liquid (*e.g.* wastewater and contaminated groundwater) and gaseous streams (*e.g.* VOC emission), and finally (e) there is a potential to utilize solar energy as reported in this particular work.[3–5] Most photodegradation is still accomplished by exposure to UV radiation although UV sources consume considerable amount of energy. Recent trends in photocatalysis research are heading towards the visible light catalysis domain. Asahi *et al.*[6] reported that nitrogen doped titania possesses visible light photocatalytic activity and photodegrades methylene blue and acetaldehyde. Anpo *et al.*[7] used ion implantation to perform doping on a series of transition metals such as V, Cr and Ni into titania films leading to the band gap shifting of titania to the visible light spectrum. In fact, all the previous studies have indicated that both TiO_2 and ZnO have a wide band-gap that can be easily achieved through UV irradiation. However, for the visible spectrum the band gap needs to be modified through band bending by using different dopants or by introducing crystal defects as a function of the nano-structuring process.[8–11] Further, it has been reported that ZnO has a higher photocatalytic efficiency compared to TiO_2 in the degradation of several organic contaminants in both acidic and basic media, which has attracted researchers to explore the properties of zinc oxide in many photocatalytic reactions.[12–14] The biggest advantage of ZnO compared with TiO_2 is that it absorbs over a larger fraction of the light spectrum and absorbs more light quanta than TiO_2.[15,16] The photocatalytic activity studies of other semiconductors such as SnO_2, CdS, WO_3, In_2O_3, ZrO_2 and ZnO

Microsystems Fabrication Laboratory, Department of Mechanical Engineering, Indian Institute of Technology Kanpur, U.P.-208016, India. E-mail: bhattacs@iitk.ac.in

† Electronic supplementary information (ESI) available. See DOI: 10.1039/c5ra10456d

‡ Contributed equally.

have been undertaken by various research groups.[17–26] The current study is more application oriented where we describe a perforated water filtration membrane with the zinc oxide as pinned nano-brushes standing upright from the surface of this membrane.

The mechanism for the photocatalytic activity of such ZnO tall nanostructures is fairly well known.[27,28] Most researchers have earlier used ZnO in a nano-powder form dispersed in industrial water for the photo-degradation of organic pollutants. However, there is an additional requirement of this method to re-filter such water, which imposes the additional constraints of achieving pure water samples due to the difficulty of re-filtering these nano-sized components.[29,30] In fact, a variety of initiatives have been ongoing to tag such nano-particles with magnetic materials and then drag the particles through the water sample to remediate the dissolved organic pollutants.[31] This also poses an additional constraint of high turbidity and reduced depth of photon penetration primarily owing to the slow settling rates of the dispersed nano-phase.

The thin-film technique appears to have lots of potential in photocatalytic applications although the diffusion limitations prevent the laminar boundary layer from getting disrupted. Our fabrication technique involves templating the ZnO tall nanostructures so that they orient in a pinned upside manner, carpeting a micro patterned film over an aluminium thin sheet (thickness 1 mm). This results in a filter which can be immersed inside the fluid which flows across the perforated membrane and this element removes the possible diffusion restrictions as in the case of thin solid films of catalyst materials. The validation of this filter membrane has been performed through photocatalytic dye degradation and we have observed a significant rise in efficiency of photodegradation using a solar spectrum.

2. Materials and methods

In order to fabricate the pinned standing nanostructures, the chemical reagents used are PGMEA (propylene glycol methyl ether acetate, M/s Sigma-Aldrich, CAS no. 484431-4L), PPG (polypropylene glycol, M/s Sigma-Aldrich, CAS no. 25322-69-4) (molecular weight: 20 000 g mol^{-1}) and PMSSQ (SGR650F, M/s Techmiglon, CAS no. 68554-70-1). The chemicals are mixed using methods as detailed below and the zinc oxide nanoseed particles are dispersed into the mixture. The nanoseeds are formulated using zinc chloride (M/s SDFCL, India) and isopropyl alcohol (M/s SDFCL). The dispersion of the solution is carried out by using ultrasonication and vortexing and this solution is coated as a thin film over a planar aluminium sheet. Zinc nitrate (M/S SDFCL, India) and hexamethylene tetra amine (HMTA, M/S SDFCL, India) are utilized for vertical growth enhancement of the ZnO nanobrushes. The following detailed synthesis steps are utilized for preparation of the filter membrane.

2.1 Fabrication of ZnO nanoseeds

ZnO nanoseeds are synthesized with the help of zinc chloride (M/s MERCK Specialties Pvt. Ltd.) (0.5 M in 10 mL isopropanol) and NaOH pellets (M/s SAMIR TECH-CHEM Pvt. Ltd., India) (0.25 M) which are properly mixed while stirring. This solution is filtered using 0.45 μm micro-syringe filters (M/s Millipore) and applied in a drop wise manner on a pre-cleaned silicon substrate. This deposited film is heated to ~200 °C and held at this temperature for a few seconds. This process is repeated several times to ensure the formation of a uniform seed layer on the substrate surface. At 200 °C, the zinc chloride crystals decompose to formulate ZnO seeds.[27,28] The seeds are extracted from the surface by scratching them into a powder and retaining for the next step.

2.2 Fabrication of ZnO nanowires and a water filtration system

In order to synthesize dense ZnO nanobrushes, poly-methyl silsesquioxane (PMSSQ) nanoparticles are initially mixed with poly-glycol methyl ether acetate (PGMEA) (1 : 5 weight ratio) and homogenized through ultra-sonication. This solution is further mixed into an already prepared PPG–PGMEA solution (1 : 1 weight ratio). 5 g of this newly prepared solution is again mixed with the scratched ZnO powder (0.1 g) as described in Section 2.1 earlier. A small part of the final solution is extracted using a hypodermic syringe, and is poured in a drop-wise manner through an end filter (0.45 μm sieve) (M/s Millipore) onto the substrate until a uniform deposition is observed over the substrate. The deposited film is heated above the decomposition temperature of PPG (>200 °C) causing evaporation. The thermal decomposition and subsequent removal of the PGMEA and PPG phase causes entropic disturbances within the dispersed nanoparticles (both PMSSQ and ZnO) eventually leading to particle–particle cross linking and a heterogeneous distribution of the ZnO nanoparticles within the PMSSQ matrix at variable heights from the base of the film. This highly seeded matrix is utilized as a template to instigate the growth of the ZnO vertical nano-structures. The seeded substrate is placed upside down in the solution made up of (0.01 M) $Zn(NO_3)_2$ and (0.05 M) HMTA in DI water (500 mL) and kept inside a gravity fed convection oven at 90 °C for over 24 hours. The chemical reaction which occurs inside the solution initiates with hydrolysis of HMTA in water releasing HCHO and NH_3. NH_3 is slowly released and assists in the formation of hydroxyl ions which leads to the minimization of bulk nucleation of Zn^{2+} in solution. This film is developed over an aluminum sheet (thickness ~ 1 mm) with an imprinted array of perforations formed earlier on the aluminum through an electro-discharge machining process (Ezee drill, M/s Ratnaparkhi Electronics). The diameters of the holes formed were 500 microns and the centre to centre distance of these holes in the array was around 2 mm.

2.3 Photocatalytic study

The photocatalytic efficiency of the synthesized ZnO nanobrushes and nanopowders was tested by measuring the photocatalyzed degradation rate of the organic dye, methylene blue (M/s Sigma-Aldrich) in aqueous solution using sunlight. Samples of degraded dye solutions were taken after various time intervals and their absorbances were measured by a UV-visible

spectrophotometer (Thermo Scientific™ Evolution 300) to evaluate their concentration change, *i.e.* the degradation rate of the dye.

2.4 Experimental set-up for thin film photocatalysis

To evaluate the photocatalytic property of the ZnO thin film and for verifying the results of theoretical modelling, 200 mL aqueous solution of methylene blue (MB) of concentration 17.5 mg L^{-1} was kept in a Petri dish along with an immobilized thin film of ZnO on a plain silicon substrate without any perforations. The total deposited mass of ZnO on the substrate was 144 mg. Slow manual stirring of the solution was performed at regular intervals. The set-up was kept beneath sunlight of an average solar intensity of 110 mW cm^{-2} which was calculated latitude/longitude-wise and timewise at the place of experiment [http://pveducation.org/]. The sample measurements were taken at time $t = 0$ and then after every subsequent 30 minutes under the solar exposure. Fig. 1 is a schematic describing the actual experiment.

2.5 Experimental set-up for the photocatalytic water remediation system

For making thin-film photocatalysis more effective, a semiconductor based photocatalytic water filtration element is synthesized. It is a known fact, that adsorption and diffusion play major roles in photocatalysis in thin-film photodegradation, and a constant volume of aqueous solution can form a stagnant boundary layer near the catalyst surface which can reduce the rate of adsorption and diffusion. To fix this issue an array of microholes were drilled on the substrate where the zinc oxide was pinned and upstanding nanostructures were realized at a later stage. This ensured that there was proper water circulation through the catalyst as coated on the perforated filter membrane and thus the boundary layer based diffusion limitations were no longer applicable for such a system. Fig. 2 shows the schematic of a complete set-up of the water filtration system with a pair of such filter membranes completely immersed in the polluted water sample. Further, the membranes were made to stand in a vertical direction exposing the maximum portion of the water sample to the filter membrane. 200 mL aqueous solution of methylene blue (MB) of concentration 20 mg L^{-1} was prepared to study the degradation of the dye in the water sample. The total deposited mass of the photocatalyst (ZnO) on both filter membranes was around 120 mg. Slow stirring of the solution was performed at regular intervals to ensure complete circulation of the water sample through the filter elements.

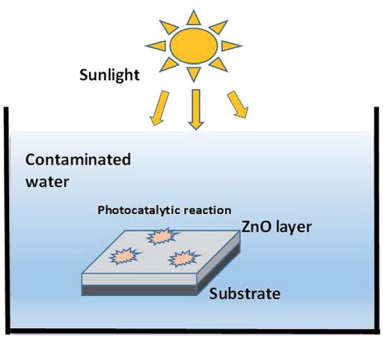

Fig. 1 The experimental set-up schematic for photocatalytic degradation with the ZnO thin film.

3. Theoretical modelling

This theoretical study incorporates the mechanisms involved in the photocatalytic degradation of the organic dyes in a thin-film catalyst. The model mainly focuses on the transport and degradation of the initial contaminants. However, the by-products of a photocatalytic reaction can affect the behaviour of the reaction but analysis of these disturbances and effects are beyond the scope of this study. Fig. 3 shows the descriptive conceptual model for degradation by the continuous thin-film ZnO photocatalyst. The aim of this study is to express the time of degradation of the continuous thin film, reaction rate constant and then to extrapolate the methodology to express the parameters for the perforated filter membrane.

Fig. 3 shows that a thin layer of the ZnO catalyst is deposited on a silicon substrate acting as an inert carrier or support. This thin-film on a carrier assembly is dipped in the organic dye aqueous solution while the whole set-up is being exposed to sunlight (110 mW cm^{-2}). The intensity of the light rays weaken as they penetrate through the ZnO layer. The attenuation caused by the solution is assumed to be insignificant compared to attenuation by the thin film catalyst. Dye molecules migrate and diffuse into the catalyst. The diffused dye molecules are degraded photocatalytically by radicals generated inside the catalyst films by the photon irradiation process. The above mentioned sequence of events explain the concentration profile

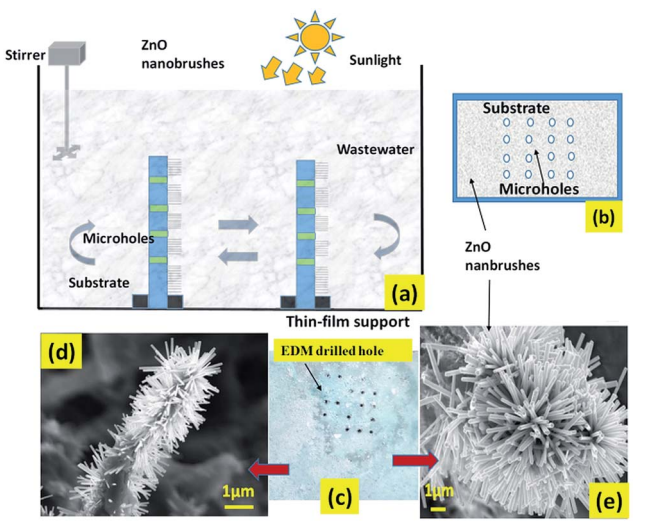

Fig. 2 (a) The schematic layout of the filter membranes, (b) microhole array based substrate over which the film has been deposited and (c) the fabricated modified thin-film catalyst with FESEM images as shown in (d) and (e).

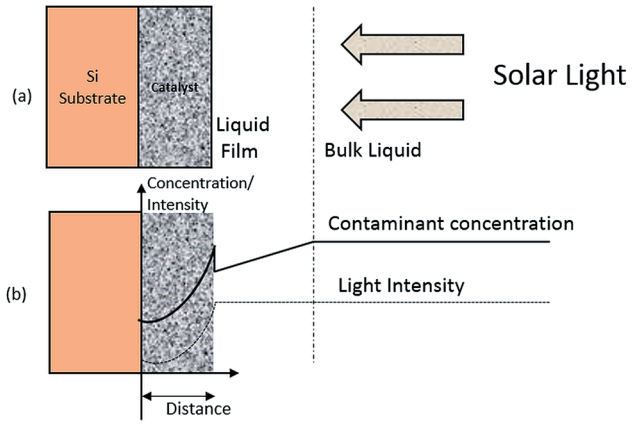

Fig. 3 The conceptual model for photo-degradation in a thin-film catalyst; (a) system configuration and (b) coordinate system and concentration profile.

of contaminants and intensity profile of solar light in the catalyst.

A Cartesian coordinate is defined in the thin-film catalyst to describe the concentration and intensity profile. The origin of the coordinate is located at the surface ($z = 0$) of the substrate. The diffusion and photocatalytic reaction rate of the organic dye into the thin film catalyst can be described by following equation.

$$\frac{\partial c}{\partial t} = D\,\frac{\partial^2 c}{\partial z^2} - kc^n S^m \quad 0 \le z \le T \tag{1}$$

In eqn (1), "c" is the adsorbed concentration of organic contaminants in the catalyst (mg g^{-1}), "D" is the diffusivity of contaminants in the catalyst (cm^2 per day), "k" is the reaction rate constant for the photodegradation reaction, "S" is the intensity of light irradiated on the catalyst (W cm^{-2}), "T" is the thickness of catalyst (cm), "t" is the reaction time (s), and m and n are reaction order constants. As represented in eqn (1), the diffusion of molecules is represented by Fick's second law.[32] The last term on the right hand side describes the photo-degradation of the organic dye. The rate of reaction is taken to be proportional to m^{th} order of intensity (S) of light and n^{th} order of adsorbed contaminant concentration (c).

Previous studies have shown that photocatalytic degradation is initiated by the adsorption of molecules on the catalyst surface.[30,33] This adsorption can form a single layer of molecules on the surface and this is depicted as a kink in the concentration of organic molecules in Fig. 3. The Langmuir–Hinshelwood (L–H) isotherm, which is developed on the basis of single layer coverage of molecules can be utilized to describe this kink step.

$$c_{|z=T} = \frac{c_{\max}\, bC_{\mathrm{w}}}{1 + bC_{\mathrm{w}}} \tag{2}$$

Eqn (2) shows the adsorbed and liquid phase concentration (C_{w}) of contaminant molecules on the catalyst surface. $c_{\max}$ (mg g^{-1}) and b (L mg^{-1}) are the coefficients for the Langmuir–Hinshelwood isotherm. $c_{\max}$ represents the maximum adsorption capacity when a complete monolayer is formed. C_{w} denotes the liquid phase concentration on the catalyst surface.

The attenuation of incident light in the catalyst is described by the Beer–Lambert expression[34] that follows an exponential decay law.

$$S = S_0 \times 10^{-\alpha(T-Z)}\ 0 < z < T \tag{3}$$

S_0 is the intensity of irradiated light (W cm^{-2}) and α is the attenuation coefficient for incident light in the catalyst (cm^{-1}).

Eqn (1)–(3), describe the basic mechanisms involved in the process of photodegradation of organic dyes in a thin-film catalyst. Organic molecules diffuse from the bulk liquid into the catalyst. This migration flux can be described using Fick's first law.[32]

$$\frac{\mathrm{d}C_{\mathrm{b}}}{\mathrm{d}t} = -\frac{A}{V}k_{\mathrm{f}}(C_{\mathrm{b}} - C_{\mathrm{w}}) \tag{4}$$

In eqn (4), "A" is equal to the exposed surface area of thin-film catalyst (cm^2), "V" is the volume of solution (cm^3), and "k_{f}" is the coefficient of film-transfer across the boundary layer (cm s^{-1}). "C_{b}" denotes the concentration in bulk liquid. To completely describe the photocatalytic performance, two initial conditions (ICs) and two boundary conditions (BCs) are mentioned in eqn (5)–(8) as follows:

$$\text{IC1: } C_{\mathrm{b}} = C_0 \text{ at } t < 0 \tag{5}$$

$$\text{IC2: } c = c' \text{ at } t < 0 \tag{6}$$

$$\text{BC1}: \frac{\partial c}{\partial z}(\text{at } z = 0) = 0 \quad t > 0 \tag{7}$$

$$\text{BC2}: \rho_{\mathrm{f}}\, D\,\frac{\partial c}{\partial z}\,(\text{at } z = T) = k_{\mathrm{f}}(C_{\mathrm{b}} - C_{\mathrm{w}}) \quad \text{at } t > 0 \tag{8}$$

"C_0" and "c'" are the initial concentrations of organic molecules in the bulk liquid and catalyst, respectively. "ρ_{f}" is the density of the thin-film ZnO catalyst (g cm^{-3}). BC1 is a no-flux condition at the catalyst–substrate interface. BC2 specifies the continuity of mass flux on the liquid–catalyst interface. Eqn (1)–(8) establish the basis of a theoretical model for the photocatalytic reaction in a thin-film ZnO catalyst. The equations were solved numerically using a combination of the orthogonal collocation method (OCM)[35] and numerical extrapolation (Euler method).[36] The solutions from the methods mentioned above provide reasonable results which are verified against the experimental data.

In order to obtain a set of normalized equations, the dimensionless variable z^* is introduced,

$$z^* = \frac{z}{T} \quad \text{for } 0 \le z^* \le 1 \tag{9}$$

The dimensionless variable z^* was substituted into eqn (1)–(8) to obtain a set of normalized equations. Subsequently, an orthogonal polynomial was selected to approximate the concentration of contaminant and the symmetrical concentration profile with respect to $z^* = 0$, which suggested a symmetrical Legendre polynomial. It has been shown that six internal collocation points can yield accurate results for diffusional problems.[37] Hence a sixth order Legendre polynomial is selected for this study.

The application of OCM resulted in the replacement of the first and second derivatives with collocation matrices **A** and **B**, respectively. The coordinate z^* was also replaced by collocation point X_i. The dimensionless equations for the photocatalytic model are presented as follows.

$$\frac{dc_i}{dt} = \frac{D}{T^2}\sum_{j=1}^{NR} B_{i,j}c_j - kS_i{}^m c_i{}^n \quad \text{for } i = 1, \ldots, N \tag{10}$$

$$c_{NR} = \frac{c_{max} b C_w}{1 + bC_w} \tag{11}$$

$$S_i = S_0 \times 10^{-\alpha H(1-X_i)} \text{ for } i = 1, \ldots, NR \tag{12}$$

$$\text{IC2: } = c_i = c_0 \text{ for } i = 1, \ldots, NR \tag{13}$$

$$\text{BC2 : } \frac{\rho_f D}{T}\sum_{j=1}^{NR} A_{NR,j}c_j = k_f(C_b - C_w) \tag{14}$$

The equation for bulk concentration eqn (4) is not changed because it is not dependent on the z variable. Boundary condition (BC1) on the carrier surface as shown in eqn (7) is satisfied automatically by the Legendre polynomial and hence eliminated safely. In the above equations, N is the number of internal collocation points, which is 6 in this study. Collocation point $i = NR\ (= N + 1)$ is located on the surface of the thin film. Eqn (11) is now rearranged as follows:

$$C_w = \frac{c_{NR}}{(c_{max} - c_{NR}) \times b} \tag{15}$$

Eqn (15) is substituted into eqn (14), and then rearranged to get an implicit equation for q_{NR}. It is solved to get c_{NR} and then using c_{NR}, C_w was calculated from eqn (15). The values of c_{NR} and C_w obtained are then substituted in eqn (4) and eqn (10) during numerical integration by Euler's method.

The numerical integration provides the concentration of contaminant in the catalyst (c_i) and in the bulk liquid (C_b). Now the mass of molecules adsorbed (M_q) is obtained from solid phase concentration (c) by integrating using a quadrature in OCM as shown below.

$$M_q = A \times T \times \rho_f \times \sum_{j=1}^{NR} (\mathbf{W}_j \times c_j) \tag{16}$$

In eqn (16), "**W**" is a vector of the weights for the numerical quadrature. The mass of molecules removed by the photocatalytic reaction is calculated by subtracting the mass adsorbed and the mass remaining in the bulk liquid from the initial mass. The above described model is applicable to thin-film catalysts. An increase in the effective surface area of the substrate owing to the array of microholes on the substrate can be incorporated as follows:

Let us define a parameter, hole area density, $p = ra/A$, where r is the number and a is the area of microholes respectively, and A denotes area of substrate.

Since the microholes are cylindrical in nature, the effective area available to exposure can be defined as:

$$A_{eff} = A\left(1 - p + 2hp\left(\frac{\pi}{a}\right)^{0.5}\right) \tag{17}$$

where, h is the thickness of the substrate. In the above equation, the second term on the right hand side denotes the area loss due to the array of holes and the third term denotes the gain in surface area. The term A used in the eqn (4) has to be replaced by A_{eff} and the modification due to the microhole array can be seen in the diffusion flux equation as follows:

$$\frac{dC_b}{dt} = -\frac{A_{eff}}{V}k_f(C_b - C_w) \tag{18}$$

Using the above equation for migration flux, variation of the fraction adsorbed with microhole density can be tracked. The solution for the above described model is coded in MATLAB (v.2013, Licensed, IIT Kanpur).

4. Results and discussion

4.1 Characterization

4.1.1 Structural characterization. Fig. 4 shows some representative FESEM images (FESEM, Quanta 200, Zeiss, Germany), taken in different zones and at various magnifications, of the vertically growing zinc oxide one-dimensional structures pinned into the nanostructured carpets. To visualize the length of the one-dimensional like structures, the SEM stage is inclined at 45 degrees and lengthways images of the wires are captured. Fig. 5(a) represents an EDAX analysis showing the presence of the elements, (Fig. 5b) shows the weight percentage of elements and (Fig. 5c) depicts the peaks corresponding to the elements present in the nanobrushes.

4.1.2 Fourier transform infra-red spectroscopy (FTIR). An FTIR spectrum of ZnO nanobrushes is presented in Fig. 6. The peak observed at ~480 cm^{-1} corresponds to the ZnO stretching vibrations. The wide peak in the range of 3300 to 3500 cm^{-1} is attributed to water molecules present in the sample. The two peaks at ~1500 cm^{-1} and ~1600 cm^{-1} are attributed to symmetric and asymmetric carboxylate bonds vibrations respectively.[38]

4.1.3 X-ray photoelectron spectroscopy (XPS). The XPS (model no. PHI 5000 Versa Prob II, FEI Inc) wide scan spectral results of ZnO nanobrushes are presented in Fig. 7. The elements with their molecular orbitals are denoted with the corresponding peaks. The peaks for Zn, C and O are analyzed further with narrow scan XPS spectral results.

The appearance of the peaks corresponding to Zn(2p), C(1s) and O(1s) is presented in Fig. 8 with narrow scan XPS results. The curve fitting shows that the Zn(2p) spectrum shows a peak at ~1021 eV, which corresponds to zinc metal present in ZnO. The C(1s) spectra show two peaks at 284 and 289 eV which are assigned to carbon in C–C and O–C=O bonds.[39–41] The O(1s) spectral peak at 531 eV may represent SiO_2 linkages (possibly because of polymethyl silsesquioxane PMSSQ) or metal oxides (ZnO). The atomic percentage from the XPS spectral results shows the element percent of Zn as 19.9%, C as 18.8%, and O as 61.3%.

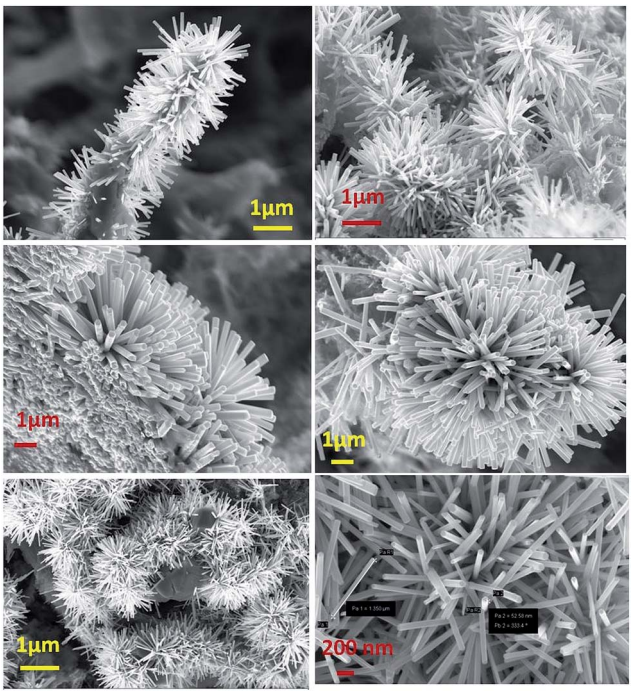

Fig. 4 A FESEM image of the fabricated nanobrushes.

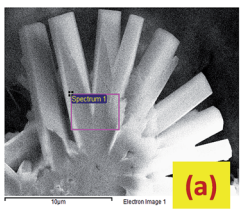

Element	Weight%	Atomic%
C K	5.88	16.03
O K	23.88	48.83
Zn K	70.23	35.14
Totals	100.00	

(b)

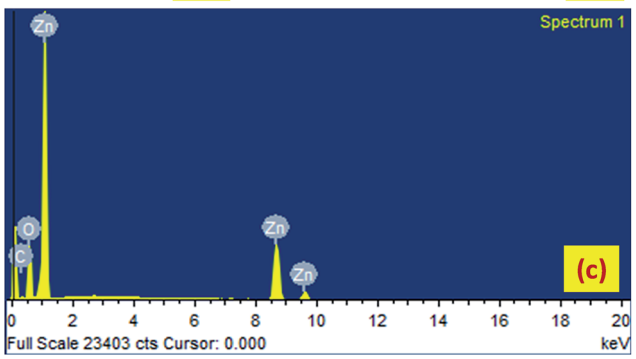

Fig. 5 (a) The analyzed area for the EDAX analysis. (b) The weight percentage of elements, and (c) the peaks which correspond to the elements present in the nanobrushes.

4.1.4 X-ray diffraction. The XRD pattern of the fabricated ZnO nanobrushes is shown in Fig. 9. All the peaks could be safely indexed as ZnO wurtzite structure as found in the standard reference data (JCPDS S6-314). Diffraction peaks corresponding to (100), (101) and (002) are observed in the XRD pattern, showing the growth of ZnO crystallites along different directions.[38] Strong preferential growth is observed along the

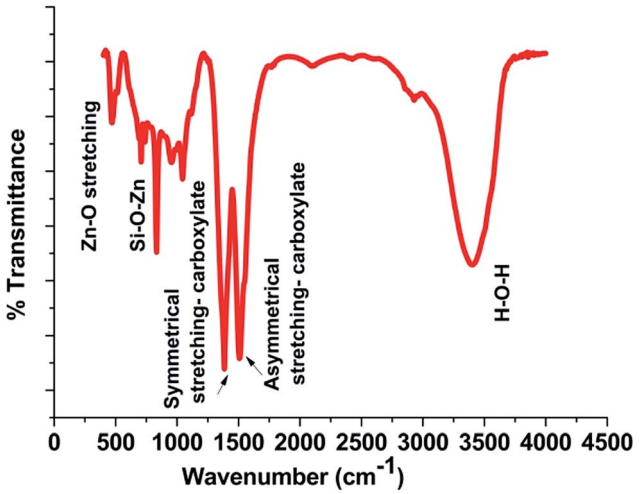

Fig. 6 FTIR spectrum of the film.

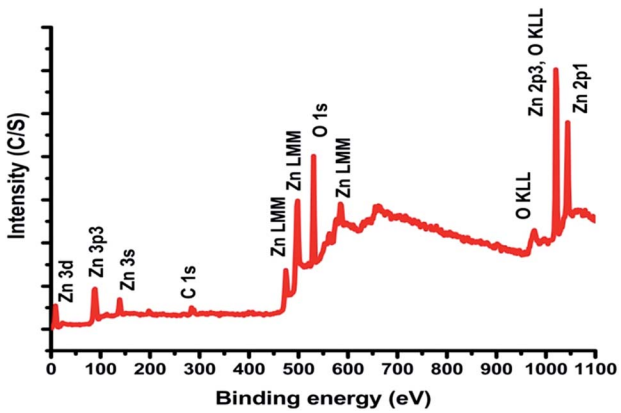

Fig. 7 XPS plot for the ZnO brush based film.

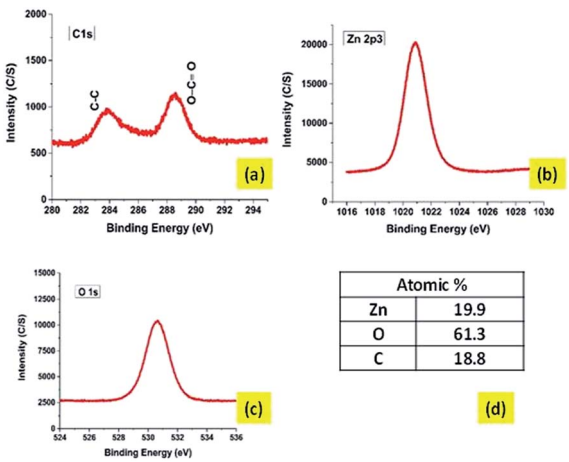

Atomic %	
Zn	19.9
O	61.3
C	18.8

(d)

Fig. 8 The narrow scan XPS results in which (a), (b) and (c) represent elements C, Zn and O respectively and (d) denotes the atomic percentages of these elements.

(002) plane indicating that the brushes are oriented vertically. This ensures the discontinuance of the laminar boundary layer.

4.2 Photocatalytic performance of the thin-film catalyst

Fig. 10(a) shows the UV-vis adsorption changes of MB in the presence of the ZnO thin-film catalyst under sunlight irradiation (110 mW cm^{-2}). Three absorbance peaks at 243, 286 and 664 nm can be observed from the UV-vis absorbance spectrum of the MB solution. The peaks at 243 and 286 nm are attributed to the absorbance of $\pi \rightarrow \pi^*$ transitions, while the peak at 664 nm is attributed to the absorbance of $n \rightarrow \pi^*$ transitions.[42] According to the changes of the absorbance intensity at 664 nm, the decolorization of MB solutions occurs in the presence of the ZnO thin film after 2.5 h and the photocatalytic reaction achieved an efficiency of 95%.

Fig. 10(b) shows that the model used for this study simulates the degradation of MB dye in sunlight reasonably well. It shows that the key mechanisms involved in the photocatalytic degradation in the thin film were captured in the model. These mechanisms include liquid-film transfer, adsorption, diffusion and photocatalytic degradation of organic molecules. Fig. 10(c) shows that the photocatalytic degradation of MB approximately follows first order reaction kinetics. The pseudo first order rate constant for this reaction is approximated as 0.344 h^{-1}. Further analysis of various catalytic properties *viz.*, diffusivity and thickness of the thin-film catalyst are performed with the help of this study.

The effect of molecular diffusion on the amount of dye adsorbed is shown Fig. 11(b). The fraction adsorbed increases initially with diffusivity but subsequently reaches a plateau. This is attributed to the fact that molecules can diffuse faster if diffusivity is higher. The plateau indicates a condition in which the organic molecules have fully penetrated into the catalyst so no more adsorption is possible. Fig. 11(a) shows the effect of increasing film thickness. It shows that an optimal thickness (~5 μm) exists for maximum adsorption. As reported in previous studies such as that by Tennakone *et al.*,[43] the degradation of carbofuran by a thin-film TiO_2 catalyst reached a maximum at about 20 coatings (~6 μm). In another study, Kim and Anderson[44] used a TiO_2-coated glass slide to destroy formic

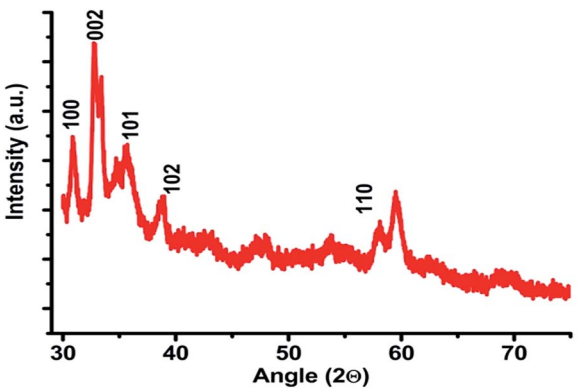

Fig. 9 The XRD plot for ZnO film.

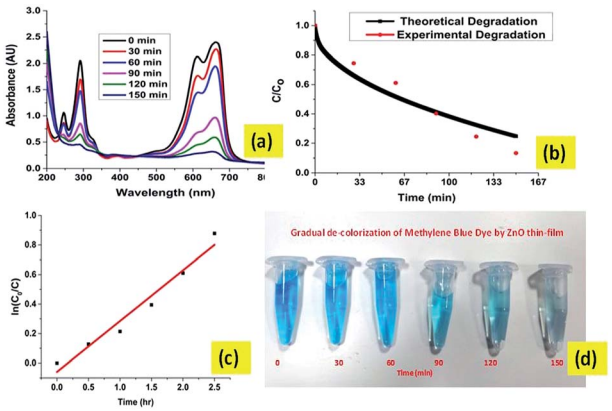

Fig. 10 The results of degradation of MB dye in natural sunlight with the ZnO thin-film catalyst. (a) UV-vis spectral plot for absorbance of MB degrading dye. (b) The theoretical and experimental data of MB degradation in the presence of sunlight. (c) Kinetics of photo-degradation of the MB dye. (d) The gradual decolourization of the MB dye by the ZnO thin-film catalyst.

acid in an aqueous solution and reported that the amount of acid destroyed increased with an increase in the number of TiO_2 coatings until a maximum was reached at 7 layers. Although it is possible that organic dye molecules are adsorbed in the interior of the thick catalyst, this can only provide a partial explanation for the effect of film thickness. It is likely that more than one factor or parameter affects the degradation of organic molecules. The effect of increased surface area due to microholes on fraction adsorbed is investigated and shown in Fig. 12. This result shows an optimum value of the diameter of the hole in order to get the maximum fraction of adsorption.

4.3 Semiconductor based photocatalytic water filtration system

Fig. 13(a) shows the UV-visible absorption spectra of samples from the photodegradation of MB dye by the water filtration system. Fig. 13(b) is a comparison of the degradation efficiency of the modified thin films with and without microholes. The total degradation time taken by the modified thin film is 45 min less than that of a thin-film catalyst for the same level of degradation. This increase in efficiency of photocatalysis can be explained as follows. The microhole array provides a pathway

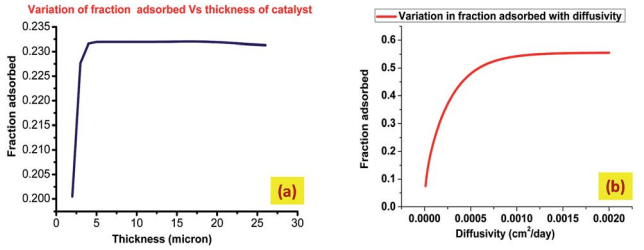

Fig. 11 Effects of catalyst properties on the amount of adsorbed fraction of contaminant. (a) The effect of varying thickness of catalyst and (b) the effect of varying diffusivity of catalyst.

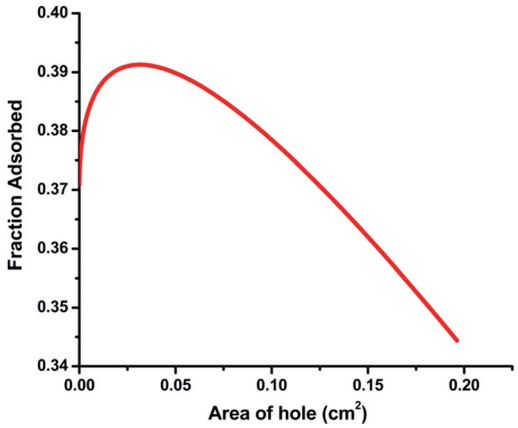

Fig. 12 The effect of variation of the hole area on the fraction adsorbed.

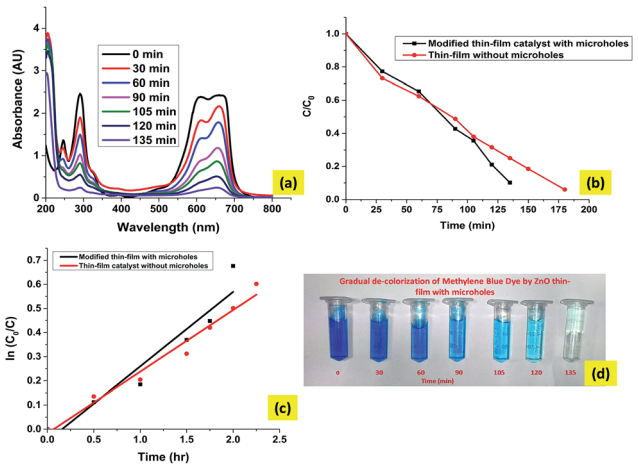

Fig. 13 The results of degradation of the MB dye with the ZnO thin-film catalyst with microholes. (a) The UV visible spectral plot for MB dye with the ZnO modified film, (b) the comparison of the microhole based film and thin film without microholes, (c) a comparison of the reaction rates of photodegradation, (d) the gradual decolourization of Mb dye with the modified thin-film catalyst.

for the circulation of solution through the catalyst which avoids the formation of a stagnant boundary layer of solution near the catalyst surface. This circulation of solution ensures that the rates of adsorption and diffusion do not fall, so high rates of adsorption and diffusion in the thin-film catalyst with microholes increase the degradation efficiency.

The first order rate constant of photocatalytic degradation for the water filtration system is 0.309 h^{-1} which is significantly higher than rate constant (0.2555 h^{-1}) for the thin-film catalyst.

5. Conclusions

In this study, we have explored the potential of solar irradiation for photocatalysis of organic dyes for water filter development purposes. The water filtration system developed in this study shows a better efficiency than traditional thin-film catalysts. A mathematical model has been developed to incorporate underlying mechanisms of the photocatalysis reaction in a thin film technique. The results obtained from the model are validated by experimental photocatalysis data. These mechanisms include liquid-film transfer, adsorption, diffusion and photocatalytic degradation of organic molecules. The model is also used to investigate the effects of catalyst properties like film thickness and diffusivity on the fraction of contaminant adsorbed on the catalyst. The results obtained from the model simulation show that there is a highly nonlinear behaviour of the catalyst properties and their adsorption efficiencies. The adsorbed fraction increases with diffusivity but after a point a plateau is reached. The results also show that an optimal film thickness exists which provides a maximum adsorption of contaminants on the catalyst surface. These results give some insight into the limiting factors in the thin film technique for photocatalysis. Thus, we have designed a filter element which increases the sample diffusion rate. This is achieved by disrupting the laminar boundary layer by diffusion through flow imposition *via* protruding nanostructures around microholes.

Acknowledgements

The authors acknowledge the financial support of the Department of Biotechnology, Food Nutrition and security group to carry out this work. They also acknowledge the help and advice provided by the staff members of the DST unit of nanoscience at IIT Kanpur for carrying out all the characterization in this work.

References

1 R. Venkatadri and R. W. Peters, Chemical oxidation technologies: ultraviolet light/hydrogen peroxide, Fenton's reagent, and titanium dioxide-assisted photocatalysis, *Hazard. Waste Hazard. Mater.*, 1993, **10**(2), 107–149.
2 M. R. Hoffmann, S. T. Martin, W. Choi and D. W. Bahnemann, Environmental applications of semiconductor photocatalysis, *Chem. Rev.*, 1995, **95**(1), 69–96.
3 A. L. Pruden and D. F. Ollis, Photoassisted heterogeneous catalysis: the degradation of trichloroethylene in water, *J. Catal.*, 1983, **82**(2), 404–417.
4 C. Kormann, D. W. Bahnemann and M. R. Hoffmann, Photolysis of chloroform and other organic molecules in aqueous titanium dioxide suspensions, *Environ. Sci. Technol.*, 1991, **25**(3), 494–500.
5 J. C. Crittenden, J. Liu, D. W. Hand and D. L. Perram, Photocatalytic oxidation of chlorinated hydrocarbons in water, *Water Research*, 1997, **31**(3), 429–438.
6 R. Asahi, T. Morikawa, T. Ohwaki, K. Aoki and Y. Taga, Visible-light photocatalysis in nitrogen-doped titanium oxides, *Science*, 2001, **293**, 269–271.
7 M. Anpo, Y. Ichihashi, M. Takeuchi and H. Yamashita, Design of unique titanium oxide photocatalysts by an advanced metal ion-implantation method and photocatalytic reactions under visible light irradiation, *Res. Chem. Intermed.*, 1998, **24**(42), 143–149.

8 H. Kyung, J. Lee and W. Choi, Simultaneous and synergistic conversion of dyes and heavy metal ions in aqueous TiO_2 suspensions under visible-light illumination, *Environ. Sci. Technol.*, 2005, **39**(7), 2376–2382.

9 Y. I. Matatov-Meytal and M. Sheintuch, Catalytic abatement of water pollutants, *Ind. Eng. Chem. Res.*, 1998, **37**(2), 309–326.

10 R. A. Nageswara, B. Sivasankar and V. Sadasivam, Kinetic study on the photocatalytic degradation of salicylic acid using ZnO catalyst, *J. Hazard. Mater.*, 2009, **166**(2), 1357–1361.

11 J. Wang, Z. Jiang, L. Zhang, P. Kang, Y. Xie, Y. Lv, R. Xu and X. Zhang, Sonocatalytic degradation of some dyestuffs and comparison of catalytic activities of nano-sized TiO_2, nano-sized ZnO and composite TiO_2/ZnO powders under ultrasonic irradiation, *Ultrason. Sonochem.*, 2009, **16**(2), 225–231.

12 M. Muruganandham and J. J. Wu, Synthesis, characterization and catalytic activity of easily recyclable zinc oxide nanobundles, *Appl. Catal., B*, 2008, **80**(1), 32–41.

13 J. C. Lee, S. Park, H.-J. Park, J.-H. Lee, H.-S. Kim and Y.-J. Chung, Photocatalytic degradation of TOC from aqueous phenol solution using solution combusted ZnO nanopowders, *J. Electroceram.*, 2009, **22**(1–3), 110–113.

14 A. A. Khassin, T. M. Yurieva, V. V. Kaichev, V. I. Bukhtiyarov, A. A. Budneva, E. A. Paukshtis and V. N. Parmon, Metal–support interactions in cobalt-aluminum co-precipitated catalysts: XPS and CO adsorption studies, *J. Mol. Catal. A: Chem.*, 2001, **175**(1), 189–204.

15 S. Chen, W. Zhao, W. Liu and S. Zhang, Preparation, characterization and activity evaluation of p–n junction photocatalyst p-ZnO/n-TiO_2, *Appl. Surf. Sci.*, 2008, **255**(5), 2478–2484.

16 S. Rehman, R. Ullah, A. M. Butt and N. D. Gohar, Strategies of making TiO_2 and ZnO visible light active, *J. Hazard. Mater.*, 2009, **170**(2), 560–569.

17 K. Vinodgopal and P. V. Kamat, Enhanced rates of photocatalytic degradation of an azo dye using SnO_2/TiO_2 coupled semiconductor thin films, *Environ. Sci. Technol.*, 1995, **29**(3), 841–845.

18 B. Neppolian, H. C. Choi, S. Sakthivel, B. Arabindoo and V. Murugesan, Solar/UV-induced photocatalytic degradation of three commercial textile dyes, *J. Hazard. Mater.*, 2002, **89**(2), 303–317.

19 S. Lathasree, A. Nageswara Rao, B. SivaSankar, V. Sadasivam and K. Rengaraj, Heterogeneous photocatalytic mineralisation of phenols in aqueous solutions, *J. Mol. Catal. A: Chem.*, 2004, **223**(1), 101–105.

20 C. Lizama, J. Freer, J. Baeza and H. D. Mansilla, Optimized photodegradation of Reactive Blue 19 on TiO_2 and ZnO suspensions, *Catal. Today*, 2002, **76**(2), 235–246.

21 A. Akyol, H. C. Yatmaz and M. Bayramoglu, Photocatalytic decolorization of Remazol Red RR in aqueous ZnO suspensions, *Appl. Catal., B*, 2004, **54**(1), 19–24.

22 M. Mahalakshmi, S. Vishnu Priya, B. Arabindoo, M. Palanichamy and V. Murugesan, Photocatalytic degradation of aqueous propoxur solution using TiO_2 and Hβ zeolite-supported TiO_2, *J. Hazard. Mater.*, 2009, **161**(1), 336–343.

23 S. K. Kansal, M. Singh and D. Sud, Studies on photodegradation of two commercial dyes in aqueous phase using different photocatalysts, *J. Hazard. Mater.*, 2007, **141**(3), 581–590.

24 S. G. Botta, J. A. Navío, M. C. Hidalgo, G. M. Restrepo and M. I. Litter, Photocatalytic properties of ZrO_2 and Fe/ZrO_2 semiconductors prepared by a sol–gel technique, *J. Photochem. Photobiol., A*, 1999, **129**(1), 89–99.

25 S. B. Sadale, S. M. Chaqour, O. Gorochov and M. Neumann-Spallart, Photoelectrochemical and physical properties of tungsten trioxide films obtained by aerosol pyrolysis, *Mater. Res. Bull.*, 2008, **43**(6), 1472–1479.

26 M. Hepel and J. Luo, Photoelectrochemical mineralization of textile diazo dye pollutants using nanocrystalline WO_3 electrodes, *Electrochim. Acta*, 2001, **47**(5), 729–740.

27 A. Gupta, S. S. Pandey, M. Nayak, A. Maity, S. Basu Majumder and S. Bhattacharya, Hydrogen sensing based on nanoporous silica-embedded ultra dense ZnO nanobundles, *RSC Adv.*, 2014, **4**(15), 7476–7482.

28 A. Gupta, K. Mondal, A. Sharma and S. Bhattacharya, Superhydrophobic polymethylsilisesquoxane pinned one dimensional ZnO nanostructures for water remediation through photo-catalysis, *RSC Adv.*, 2015, **5**, 45897–45907.

29 D. F. Ollis, Contaminant degradation in water, *Environ. Sci. Technol.*, 1985, **19**(6), 480–484.

30 D. F. Ollis, E. Pelizzetti and N. Serpone, Photocatalyzed destruction of water contaminants, *Environ. Sci. Technol.*, 1991, **25**(9), 1522–1529.

31 S. Kurinobu, K. Tsurusaki, Y. Natui, M. Kimata and M. Hasegawa, Decomposition of pollutants in wastewater using magnetic photocatalyst particles, *J. Magn. Magn. Mater.*, 2007, **310**(2), e1025–e1027.

32 J. Crank, *The mathematics of diffusion*, Clarendon press, Oxford, 1975, vol. 2, p. 3.

33 K. Vinodgopal, S. Hotchandani and P. V. Kamat, Electrochemically assisted photocatalysis: titania particulate film electrodes for photocatalytic degradation of 4-chlorophenol, *J. Phys. Chem.*, 1993, **97**(35), 9040–9044.

34 R. P. Schwarzenbach, P. M. Gschwend and D. M. Imboden, *Environmental Organic Chemistry*, Wiley, New York, 1993.

35 B. A. Finlayson, *The method of weighted residuals and variational principles*, SIAM, 2013, vol. 73.

36 J. C. Butcher, *The numerical analysis of ordinary differential equations: Runge–Kutta and general linear methods*, Wiley-Interscience, 1987.

37 J. C. Crittenden, B. W. C. Wong, W. E. Thacker, V. L. Snoeyink and R. L. Hinrichs, Mathematical model of sequential loading in fixed-bed adsorbers, *J. - Water Pollut. Control Fed.*, 1980, 2780–2795.

38 Z. R. Khan, M. Shoeb Khan, M. Zulfequar and M. Shahid Khan, Optical and structural properties of ZnO thin films fabricated by sol–gel method, *Mater. Sci. Appl.*, 2011, **2**(5), 340.

39 H. S. Hamid and F. Eric, XPS & FTIR study of adsorption characteristics using cationic and anionic collectors on smithsonite, *J. Miner. Mater. Charact. Eng.*, 2006, **5**(1), 21.

40 B. Singh, D. Velázquez, J. Terry and M. R. Linford, The equivalent width as a figure of merit for XPS narrow scans, *J. Electron Spectrosc. Relat. Phenom.*, 2014, **197**, 56–63.

41 Y. Do, J.-S. Choi, S. K. Kim and Y. Sohn, The Interfacial Nature of TiO_2 and ZnO Nanoparticles Modified by Gold Nanoparticles., *Bull. Korean Chem. Soc.*, 2010, **31**(8), 2170–2174.

42 D. Heger, J. Jirkovský and P. Klan, Aggregation of methylene blue in frozen aqueous solutions studied by absorption spectroscopy, *J. Phys. Chem. A*, 2005, **109**(30), 6702–6709.

43 K. Tennakone, C. T. K. Tilakaratne and I. R. M. Kottegoda, Photomineralization of carbofuran by TiO_2-supported catalyst, *Water Research*, 1997, **31**(8), 1909–1912.

44 D. H. Kim and M. A. Anderson, Photoelectrocatalytic degradation of formic acid using a porous titanium dioxide thin-film electrode, *Environ. Sci. Technol.*, 1994, **28**(3), 479–483.